Spin wave modelling in arrays of ferromagnetic thin stripes: application to Brillouin light scattering in permalloy

2007 J. Phys.: Condens. Matter 19 176220

(http://iopscience.iop.org/0953-8984/19/17/176220)

IOP PUBLISHING JOURNAL OF PHYSICS: CONDENSED MATTER

J. Phys.: Condens. Matter **19** (2007) 176220 (12pp) doi:10.1088/0953-8984/19/17/176220

Spin wave modelling in arrays of ferromagnetic thin stripes: application to Brillouin light scattering in permalloy

F Zighem, Y Roussigné, S-M Chérif and P Moch

Laboratoire des Propriétés Mécaniques et Thermodynamiques des Matériaux, CNRS, Institut Galilée, Université Paris-Nord, Avenue J-B Clément, 93430 Villetaneuse, France

E-mail: zighem@galilee.univ-paris13.fr

Received 2 February 2007, in final form 5 February 2007
Published 10 April 2007
Online at stacks.iop.org/JPhysCM/19/176220

Abstract

The magnetic Brillouin scattering of arrays of permalloy stripes with rectangular 29 nm $\times$ L cross section (L = 500, 1000, 1500 nm) is studied versus the amplitude and the direction of the applied magnetic field and of the transferred wavevector. A simple model provides a satisfactory agreement of the full set of experimental results: each stripe is viewed as a continuous film showing an in-plane anisotropy due to the demagnetizing effects induced by lateral surfaces. We introduce an anisotropy field $H_a = aM$, where M stands for the magnetization and where the coefficient a can be evaluated directly, at least approximately. In addition, we give an account of the previously studied magnetic mode quantization and of the observed variations in the Stokes/anti-Stokes asymmetry in patterned arrays as well as in continuous films.

(Some figures in this article are in colour only in the electronic version)

1. Introduction

In recent years many theoretical, numerical and experimental studies concerning spin waves in magnetic stripes have been performed [1–18]. Among the experimental techniques, propagating spin wave spectroscopy and Brillouin light scattering (BLS) are particularly interesting, since they can provide information about the frequency dispersion, the group velocity and the damping of magnetic excitations versus their wavevector. In the following, we present a Brillouin study of spin waves in arrays of permalloy thin stripes using various geometrical configurations for the direction of the applied magnetic field **H** and of the transferred in-plane wavevector **Q** involved in the scattering of light. We show that a rather simple approximate model quite satisfactorily gives account of the observed results. It derives from the well-known calculations related to continuous magnetic infinite thin films: the stripe structure introduces an effective anisotropy energy term connected to demagnetizing effects

and a wavevector quantization. Some consequences of this behaviour have been described previously: for instance, when **H** is applied along the stripes with **Q** perpendicular to **H**, one is faced with a quantization deduced from the dispersion of a continuous thin film for the pseudo-Damon–Eshbach configuration assuming values of the wavevector nearly equal to $n\pi/L$, where n stands for any positive integer and where L is the width of the stripes.

2. Experimental details

2.1. Studied samples

Different arrays of stripes originating from a unique continuous permalloy film were elaborated. The study of this continuous film provides a set of magnetic characteristic quantities: magnetization M, gyromagnetic factor γ, and exchange stiffness parameter A. These quantities are assumed to be unaffected by the patterning which gives rise to the arrays of stripes. This control film of thickness $d = 29$ nm was obtained by RF sputtering on a silicon substrate. The patterning, which uses a technique combining electron beam lithography and ion beam sputtering, has been described previously [19]. Three series of arrays of parallel stripes, separated by a 300 nm interval, were prepared with a width, L, of 500, 1000 and 1500 nm, respectively.

2.2. Brillouin spectra

The polarized magnetic Brillouin spectra were achieved using a tandem 2×3 Fabry–Perot interferometer illuminated by a single-mode Ar^+ ion laser at a wavelength of $\Lambda = 514.5$ nm using a power of 200 mW or less. Backscattering geometry was used, with an angle of incidence θ that could be varied, thus allowing us to monitor the wavevector transfer $Q = 4\pi \sin[\theta]/\Lambda$. The variations in the spectra versus the in-plane applied magnetic field were also studied for various geometrical configurations (e.g. $\mathbf{H} \perp \mathbf{Q}, \mathbf{Q} \perp$ stripes; $\mathbf{H} \perp \mathbf{Q}$, $\mathbf{Q} \parallel$ stripes; $\mathbf{H} \parallel \mathbf{Q}, \mathbf{Q} \perp$ stripes).

3. Results and discussion

3.1. Continuous film

In the so-called 'Damon–Eshbach' geometry ($\mathbf{H} \perp \mathbf{Q}$), the calculation of the spin wave frequencies and of the resulting shape of the Brillouin spectra is a well-known problem [20–23] and, in principle, allows us to fit the magnetic parameters. We have extended this calculation without any major difficulty to other geometrical arrangements, in particular to the so-called 'backward' geometry ($\mathbf{H} \parallel \mathbf{Q}$). Figures 1(a) and (b) provide an example of such fits for the two above-mentioned situations. It is of interest to notice that the well-known Stokes/anti-Stokes asymmetry appearing in the 'Damon–Eshbach' spectra is absent in the 'backward' ones.

Practically, the fits are derived from the frequency variations of the observed lines versus the magnetic field and versus the angle of incidence. In addition to M, γ and A, a perpendicular anisotropy related to interfacial energy is often reported. However, the experimental accuracy and the neglected damping effects do not allow a separate evaluation of $4\pi M$ and of the anisotropy field H_{an} and we can only determine $(4\pi M - H_{an})$. Our best fits, illustrated in figures 2(a)–(c), lead to $A = 1 \times 10^{-6}$ erg cm^{-1}, $\gamma = 1.87 \times 10^7$ Hz G^{-1}, $(4\pi M - H_{an}) = 7600$ G. In bulk permalloy, $4\pi M$ approaches 10 000 G; keeping this value for the thin film would results in an anisotropy field of a few kOe. However, in order to simplify the following

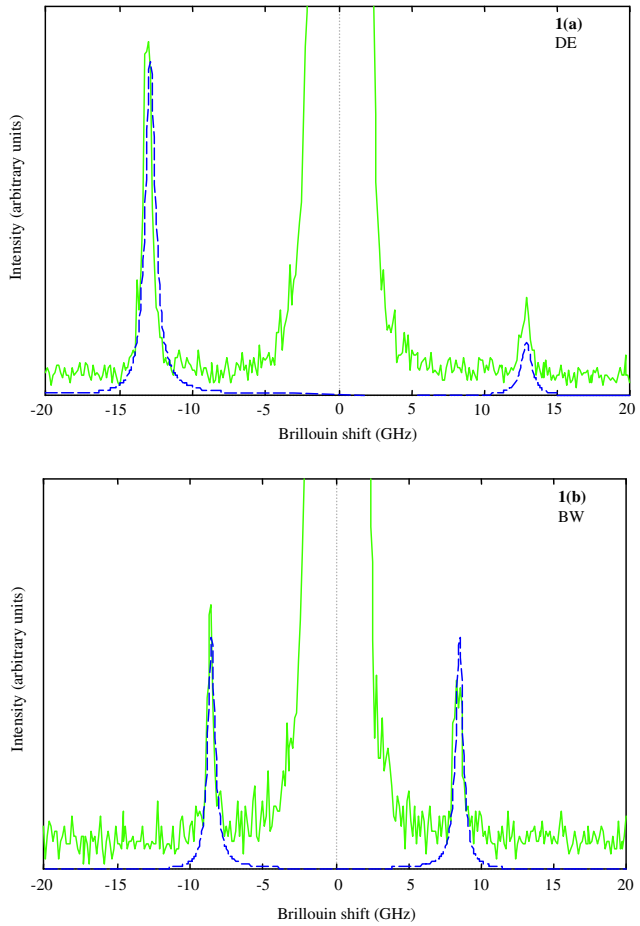

Figure 1. Examples of calculated Brillouin spectra compared to experimental results for a continuous permalloy layer in DE geometry (**H** ∥ **M** ⊥ **Q**: (a)) and in BW geometry (**H** ∥ **M** ∥ **Q**: (b)). Dashed lines: calculated spectra; full lines: experimental spectra. The calculations use: $4\pi M = 7600$ G; $\gamma = 1.87 \times 10^7$ Hz G^{-1}; $A = 1 \times 10^{-6}$ erg cm^{-1}; $d = 29$ nm; $H = 1000$ Oe (angles of incidence: $\theta = 45°$ in (a); $\theta = 36°$ in (b)).

presentation, we shall state that $4\pi M = 7600$ G, keeping in mind that M stands for an effective magnetization (sometimes called M_{eff} [24, 25]) giving account of the spin wave behaviour.

Due to the small thickness of the film, the dipolar mode is well separated from the other magnetic excitations (standing spin waves) and, when one focuses on the Brillouin spectra, its properties can be treated separately from the other modes, using a model introduced by Stamps and Hillebrands [26] and extended by Stamps [27] for the study of thin samples. This derives from the approximate linear equations monitoring the mean amplitude of the oscillatory magnetization calculated over the sample thickness. It provides explicit expressions for the spin wave frequencies, namely:

$$\left(\frac{\omega}{\gamma}\right)^2 = \left(\frac{8\pi M}{Qd+2} + H + \frac{2AQ^2}{M}\right)\left(\frac{4\pi M Qd}{Qd+2} + H + \frac{2AQ^2}{M}\right)$$

for the 'Damon–Eshbach' geometry (1)

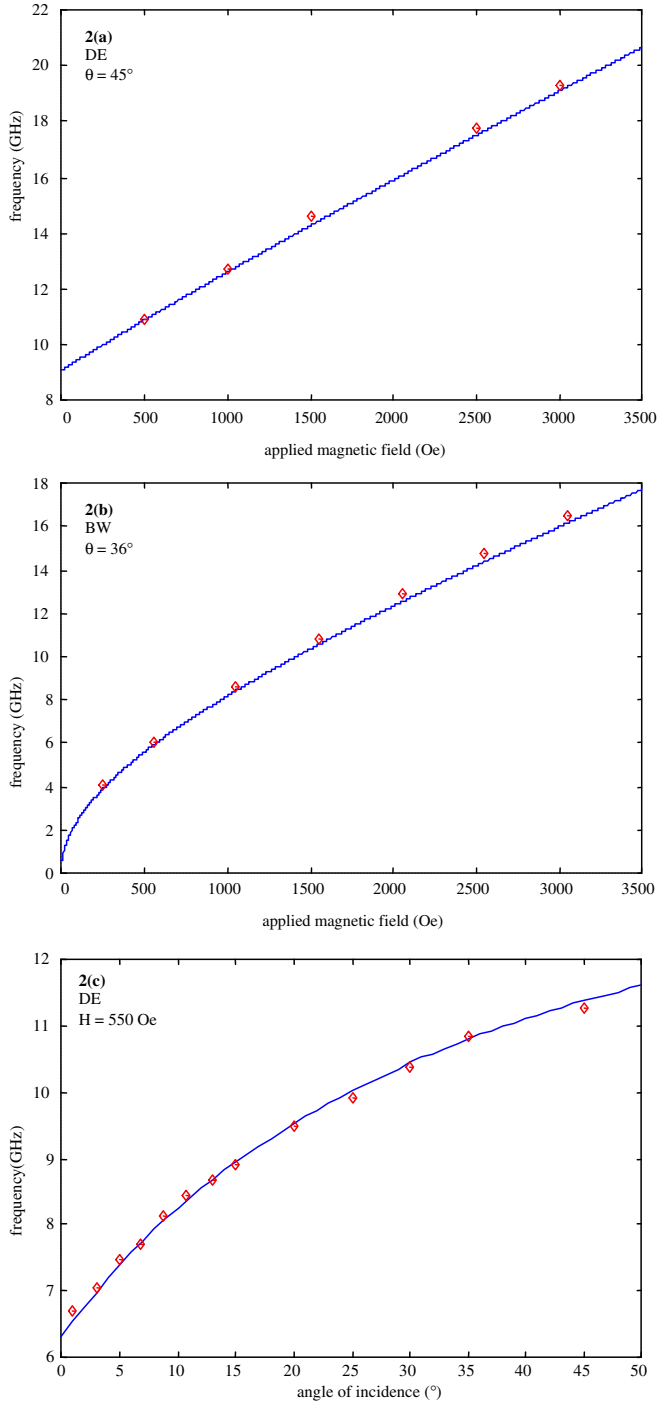

Figure 2. Best fit for the observed Brillouin frequency variations in a continuous permalloy layer: (a) versus the magnetic field in the DE geometry; (b) versus the magnetic field in the BW geometry; (c) versus the angle of incidence in the DE geometry. Full lines: calculated variations with $4\pi M = 7600$ G, $\gamma = 1.87 \times 10^7$ Hz G^{-1}, $A = 1 \times 10^{-6}$ erg cm^{-1}. Points: experimental values.

$$\left(\frac{\omega}{\gamma}\right)^2 = \left(\frac{8\pi M}{Qd+2} + H + \frac{2AQ^2}{M}\right)\left(H + \frac{2AQ^2}{M}\right)$$

for the 'backward' geometry. (2)

We have verified that the above expressions and the complete calculation provide the same frequency values within the experimental precision interval (0.1 GHz).

3.2. Arrays of stripes

The film patterning induces two consequences: (i) an in-plane anisotropy, presumably mainly related to the demagnetizing effects related to the occurrence of lateral surfaces; (ii) a quantization of the allowed wavevector related to restrictions in the translational invariance. For a complete description of the propagative spin waves, numerical calculation are needed: such an approach concerning a unique isolated stripe has previously been presented [11]. Its generalization to an infinite array is relatively heavy; on the other hand, it only provides poor insight of the physical modifications induced by the patterning. The situation can be simplified significantly assuming that each stripe suffers an additional anisotropy energy density term which, in first approximation, is written as $aM_x^2/2$, where a is some constant to adjust that depends on the geometrical arrangement of the studied array and where M_x stands for the in-plane component of the magnetization perpendicular to the direction of the stripe. The quantity aM can be viewed as an anisotropy field, and it is realistic to attempt to identify aM_x with an effective mean demagnetizing field. The evaluation of the demagnetizing field is straightforward if the magnetization is supposed to be uniform in the stripe: numerical calculations, using for instance the OOMMF program [28], show that this approximation of a uniform magnetization is reasonably good in view of the geometrical characteristics and of the applied fields used. Indeed, the demagnetizing field is not uniform inside a stripe: the appropriate effective demagnetizing field cannot be derived easily and, in the following, will be considered as an adjustable parameter. Two limits can be regarded: (i) the first one uses the value of the demagnetizing field at the centre of each stripe; it underestimates the parameter a, since it nearly corresponds to the minimum value of the demagnetizing field inside the stripe. This provides: $a = 0.31$, 0.11 and 0.06 for stripe widths 500, 1000 and 1500 nm, respectively; (ii) the second one uses the mean value of the demagnetizing field calculated over the full cross section of each stripe; it presumably overestimates the parameter a, since it is considerably influenced by the large values of the magnetizing field in the immediate vicinity of the lateral surface, which is a region that cannot satisfactorily describe the studied pseudo-dipolar modes. This provides: $a = 0.84$, 0.44, 0.29 for the stripe widths 500, 1000 and 1500 nm, respectively.

Using this model, the static magnetization of each stripe is easily found by minimizing a term of energy density, which can be written as:

$$E_0 = -\mathbf{H}\cdot\mathbf{M} + \frac{aM_x^2}{2}. \tag{3}$$

Among the above-mentioned cases studied, two very different situations have to be considered:

(i) $\mathbf{H} \parallel$ stripes ($\mathbf{z}$ axis): the magnetization remains along $\mathbf{H}$; for $|H| > H_a = aM$, $\mathbf{H}$ and $\mathbf{M}$ keep the same direction; for $|H| < H_a$, hysteresis effects can occur [12, 15].

(ii) $\mathbf{H} \perp \mathbf{z}$: $\mathbf{M}$ lies along $\mathbf{H}$ only for $|H| \geqslant H_a$; for $|H| < H_a$, the orientation of M corresponds to an 'oblique' phase ($M_x = M(H/H_a)$). A spin wave softening around the transition field H_a is then expected for specific directions of the wavevector [9, 11, 16].

Notice that, strictly speaking, for other directions a residual obliquity remains, whatever the value of the applied field.

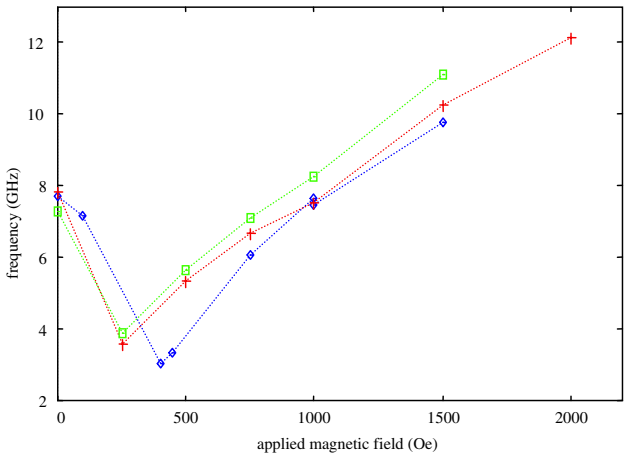

Figure 3. Experimental evidence for frequency softening in the ($\mathbf{H} \perp \mathbf{z}, \mathbf{H} \parallel \mathbf{Q}$) geometry for three arrays of stripes: $L = 500$ nm (points), 1000 nm (crosses) and 1500 nm (squares). Angle of incidence: $\theta = 30°$.

In figure 3, we have reported the frequency variations versus the field for $\mathbf{H} \perp \mathbf{z}$, as observed in the 'backward geometry' ($\mathbf{Q} \parallel \mathbf{H}$) for the three stripe widths studied: a softening clearly appears. To interpret this behaviour we use the same approach as in the preceding section, but adding the term $aM_x^2/2$ to the energy density. This model provides the following expressions for the frequency:

$$\left(\frac{\omega}{\gamma}\right)^2 = \left(\frac{8\pi M}{Qd+2} + \frac{2AQ^2}{M}\right)\left(\frac{4\pi MQd}{Qd+2}\left(1 - \frac{H^2}{H_a^2}\right) + \frac{2AQ^2}{M} + H_a\left(1 - \frac{H^2}{H_a^2}\right)\right) \quad \text{for } H < H_a \tag{4}$$

$$\left(\frac{\omega}{\gamma}\right)^2 = \left(\frac{8\pi M}{Qd+2} + \frac{2AQ^2}{M} + H - H_a\right)\left(H + \frac{2AQ^2}{M} - H_a\right) \quad \text{for } H > H_a. \tag{5}$$

This results in a softening for $H = H_a$. However, due to the exchange contribution, the frequency does not completely vanish for $H = H_a$. In figure 4, we show typical Brillouin spectra obtained in the oblique phase ($H < H_a$) and in the aligned phase ($H > H_a$): the Stokes/anti-Stokes asymmetry is absent for the aligned case, which is reminiscent of the 'backward' geometry, as is expected since the magnetization is parallel to the transferred wavevector $\mathbf{Q}$. In contrast, for $H < H_a$, a significant asymmetry is observed, due to the misalignment between $\mathbf{M}$ and $\mathbf{Q}$, which is similar to the asymmetry obtained with thin films studied in the 'Damon–Eschbach' geometry.

In figure 5, we have reported the frequency variations versus the field for $\mathbf{H} \perp \mathbf{z}$, as observed in the 'Damon–Eshbach' geometry ($\mathbf{Q} \perp \mathbf{H}$) for the stripes of width 1000 nm: softening does not appear, but a change in slope is observed at $H = H_a$, in agreement with the predictions of the model, which provides the expressions:

$$\left(\frac{\omega}{\gamma}\right)^2 = \left(\frac{8\pi M}{Qd+2} + \frac{2AQ^2}{M}\right)\left(\left(\frac{4\pi MQd}{Qd+2} - H_a\right)\frac{H^2}{H_a^2} + H_a + \frac{2AQ^2}{M}\right) \quad \text{for } H < H_a \tag{6}$$

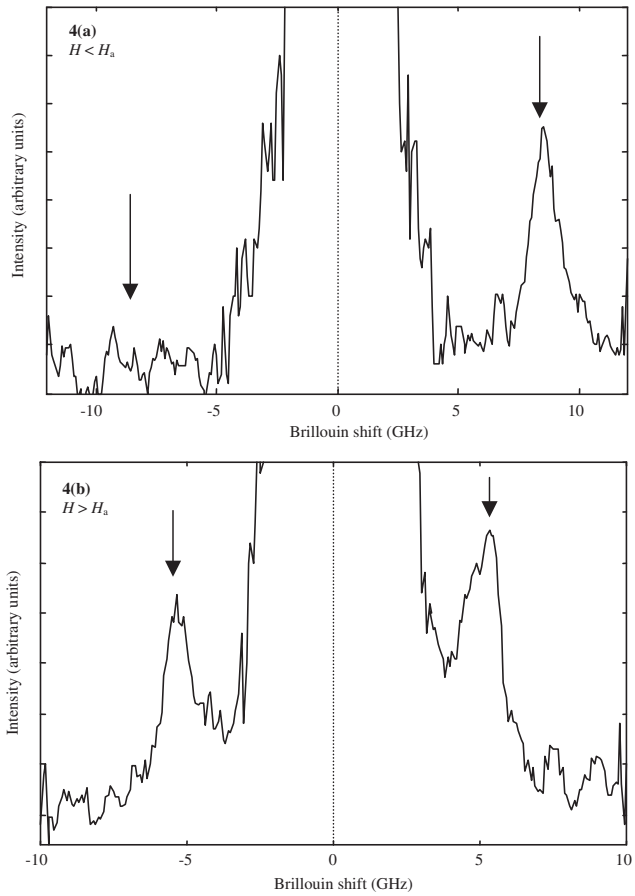

Figure 4. Two typical Brillouin spectra in the ($\mathbf{H} \perp \mathbf{z}$, $\mathbf{H} \parallel \mathbf{Q}$) geometry, obtained with H below (a) and above (b) H_a: (a) $H = 0$; (b) $H = 500$ Oe.

$$\left(\frac{\omega}{\gamma}\right)^2 = \left(\frac{8\pi M}{Qd+2} + H + \frac{2AQ^2}{M} - H_a\right)\left(\frac{4\pi MQd}{Qd+2} + H + \frac{2AQ^2}{M} - H_a\right) \quad \text{for } H > H_a. \tag{7}$$

Notice that, when $H = 0$, the non-vanishing of the frequency is related to the dynamical part of the anisotropy field.

In figure 5, we also show the frequency variations versus the field for $\mathbf{H} \parallel \mathbf{z}$, as observed in the 'Damon–Eshbach' geometry ($\mathbf{Q} \perp \mathbf{H}$) for stripes of width 1000 nm. The expected frequency is given by:

$$\left(\frac{\omega}{\gamma}\right)^2 = \left(\frac{8\pi M}{Qd+2} + H + \frac{2AQ^2}{M}\right)\left(\frac{4\pi MQd}{Qd+2} + H + \frac{2AQ^2}{M} + H_a\right). \tag{8}$$

In figure 6, we compare the experimental spectra for the stripes of width 1000 nm to the studied model for the three geometrical arrangements: the best fit is obtained for $H_a = 180$ Oe; this result corresponds to $a = 0.298$ and then lies within the above-mentioned interval [0.11, 0.44]. In figure 7, we present the obtained fits for the 500 nm and the 1500 nm widths: we find $a = 0.600$ and 0.22, which, as expected, lie in the [0.31, 0.84] and the [0.06, 0.29] intervals,

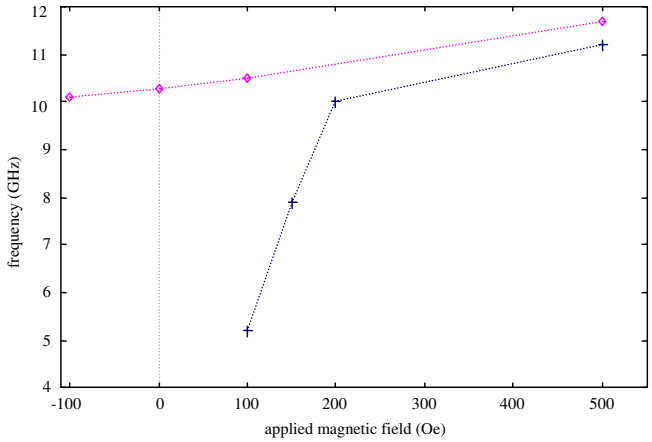

Figure 5. Frequency variations versus H in the ($\mathbf{H} \perp \mathbf{z}$, $\mathbf{H} \perp \mathbf{Q}$) geometry (crosses) and in the ($\mathbf{H} \parallel \mathbf{z}$, $\mathbf{H} \perp \mathbf{Q}$) geometry (points). $L = 1000$ nm and $\theta = 65°$.

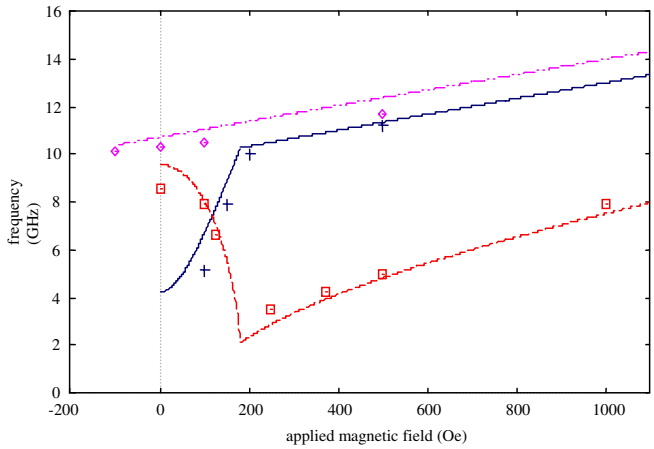

Figure 6. Best fit for the observed Brillouin frequency variations in an array of stripes ($L = 1000$ nm) in three configurations: (i) ($\mathbf{H} \perp \mathbf{z}$, $\mathbf{H} \parallel \mathbf{Q}$); calculation: dashed line, experimental: squares; (ii) ($\mathbf{H} \perp \mathbf{z}$, $\mathbf{H} \perp \mathbf{Q}$); calculation: full line, experimental: crosses; (iii) ($\mathbf{H} \parallel \mathbf{z}$, $\mathbf{H} \perp \mathbf{Q}$); calculation: dot–dashed line, experimental: points. Calculated variations with $a = 0.298$ (and $4\pi M = 7600$ G, $\gamma = 1.87 \times 10^7$ Hz G^{-1}, $A = 1 \times 10^{-6}$ erg cm^{-1}).

respectively. In addition to the above-discussed results, we performed various studies with different angles of incidence: all the obtained spectra agree with the proposed model.

Let us now discuss the quantization effects that were not accounted for above: due to the experimental precision and to the broadness of the observed Brillouin lines, these can be observed for $\mathbf{Q}$ perpendicular to the stripes, at small Q values only, i.e. at small angles of incidence, an experimental situation which was not discussed in the preceding part of this paper. In contrast, quantization effects were studied previously in the same arrays of stripes [4]. In the dipolar approximation we came to the conclusion that the usual expression for continuous films:

$$\left(\frac{\omega}{\gamma}\right)^2 = (H + 2\pi M)^2 - (2\pi M)^2 \exp[-2Qd] \tag{9}$$

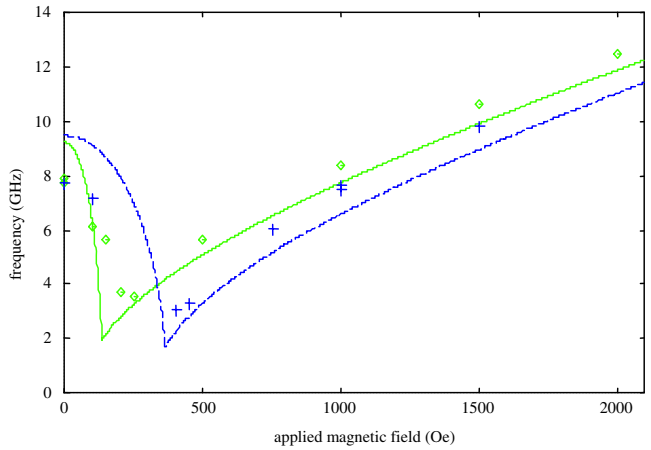

Figure 7. Best fit for the observed Brillouin frequency variations in arrays of stripes with $L = 500$ and 1500 nm in the ($\mathbf{H} \perp \mathbf{z}$, $\mathbf{H} \parallel \mathbf{Q}$) geometry: (i) $L = 500$ nm; calculation with $a = 0.600$: dashed line, experimental: crosses; (ii) $L = 1500$ nm; calculation with $a = 0.220$: full line, experimental: points.

could be used, assuming a quantization of the wavevector $Q_n = (n + \beta)\pi/L$, with $n = 0, 1, 2, 3 \ldots$ and $\beta = 2/3$. In our opinion, the anisotropy related to the demagnetizing lateral surfaces, which was not taken into account in our previous publication, is responsible of the parameter β. Expression (8), with a quantized values of the wavevector $Q'_n = n\pi/L$, is nearly equivalent to expression (9) using the wavevector:

$$Q_n = n\frac{\pi}{L} + \frac{(4\pi M + H)}{8\pi^2 M^2}\frac{H_a}{d} \tag{10}$$

(restricting us to a development to the first order). For the case studied, H can be neglected in expression (10), which becomes:

$$Q_n = n\frac{\pi}{L} + \frac{H_a}{2\pi M d}. \tag{11}$$

The above-mentioned parameter a is then given by:

$$a = 2\pi^2\frac{d}{L}\beta. \tag{12}$$

One finds $a = 0.76$, 0.38 and 0.25 for the widths 500, 1000 and 1500 nm, respectively. These values lie in the appropriate above-calculated intervals. They are slightly higher than the experimental ones reported in the present study (0.600, 0.298 and 0.22, respectively). Nevertheless, the fitting conditions were not the same: we did not introduce the exchange terms for the analysis of the quantized modes.

4. Conclusion

We have developed a simple model for the spin wave excitations in an array of magnetic stripes. In this model, a stripe is replaced by an 'ad hoc' infinite thin film described with the help of an in-plane anisotropy term: this term originates from the demagnetizing effects due to the lateral surfaces, which can be evaluated approximately. In our calculations, we also assume small relative variations in the dynamic magnetization along the direction of the thickness: we then exclude the study of the surface standing waves (SSW) related to the stripes. Moreover, this

model, which introduces a uniform effective static demagnetizing field, cannot give an account of magnetic modes confined near the edges of the stripes [7, 8]: these latter excitations present distinct behaviours, showing, for instance, softening near specific magnetic fields [11, 16].

In spite of the above restrictions, our method provides a satisfactory description of the observed magnetic Brillouin spectra of different arrays of magnetic stripes studied with a large variety of geometrical arrangements and of applied magnetic fields.

This method can be used in many experimental situations. The only requirements are: (i) that the static magnetic quantities are uniform; (ii) that the dynamic quantity slightly varies over the thickness. There is no need to assume any given profile of the dynamic magnetization. The form of the energy density can be modified and includes additional terms of anisotropy and/or bias interfacial exchange.

Appendix. Expression of the spin wave frequencies

A thin stripe is regarded as an infinite layer showing anisotropy induced by the demagnetizing field: assuming a uniform in-plane static magnetization of amplitude M, its direction is obtained by minimizing the following energy density term:

$$E = -H_x M_x - H_z M_z + H_a M_x^2/2M \qquad \text{with } M_x^2 + M_z^2 = M^2 \tag{A.1}$$

where z labels the direction along the stripe, and x defines the direction of its width. $H_a = aM$ can be estimated from the demagnetizing field calculated for a lattice of stripes saturated along its hard in-plane axis (see main text above).

The conditions of minimization can be written:

$$H_x - H_a M_x/M = \lambda M_x, \qquad H_z = \lambda M_z \qquad \text{with: } M_x^2 + M_z^2 = M^2. \tag{A.2}$$

(i) If $H_z \neq 0$, λ is obtained through the relation:

$$(H_z/\lambda)^2 + (H_x/(\lambda + H_a/M))^2 = M^2. \tag{A.3}$$

(ii) If $H_z = 0$, then $\lambda M_z = 0$:

$$\text{either } H_x < H_a \text{ and } \lambda = 0, \qquad \text{or} \qquad H_x > H_a \text{ and } M_z = 0. \tag{A.4}$$

The dynamical magnetization and, consequently, its averaged value $\langle \mathbf{m} \rangle$ over the film thickness, is governed by the Landau–Lifshift equation, which provides:

$$\mathrm{i}(\omega/\gamma)\langle \mathbf{m} \rangle = \mathbf{M} \times \langle \mathbf{h}_{\text{eff}} \rangle + \langle \mathbf{m} \rangle \times \mathbf{H}_{\text{eff}} \tag{A.5}$$

where $\langle \mathbf{h}_{\text{eff}} \rangle$ is the averaged dynamic magnetic field and where $\mathbf{H}_{\text{eff}} = \lambda \mathbf{M}$; ω is the radial frequency.

We will show below that the frequency of a propagating eigenmode of wavevector $\mathbf{Q} = Q_x \mathbf{x} + Q_z \mathbf{z}$ of amplitude Q is obtained using the relation:

$$\begin{aligned}(\omega/\gamma)^2 = {} & (8\pi/(Qd+2) + \lambda + 2AQ^2/M^2)(4\pi d(Q_x M_z - Q_z M_x)^2/(Q(Qd+2)) \\ & + (\lambda + 2AQ^2/M^2)M^2 + M_z^2 H_a/M)\end{aligned} \tag{A.6}$$

where d is the thickness of the film and where A is the exchange stiffness. Expression (A.6) reduces to equations (4)–(8) related to the geometrical arrangements described in the main text.

The proof of equation (A.6) starts from the expression of the dynamic effective magnetic field:

$$\mathbf{h}_{\text{eff}} = \mathbf{h} + (2A/M^2)\Delta \mathbf{m} - (H_a m_x/M)\mathbf{x} \tag{A.7}$$

where, in the quasi-static approximation, the usual dynamic demagnetizing field $\mathbf{h}$ can be written as

$$\mathbf{h} = \nabla \varphi. \tag{A.8}$$

The potential φ is related to $\mathbf{m}$ by:

$$\Delta\varphi + 4\pi\nabla\cdot\mathbf{m} = 0. \tag{A.9}$$

It results from (A.8) and (A.9) that:

$$\mathbf{H} = \mathrm{i}(Q_x\mathbf{x} + Q_z\mathbf{z})\varphi + \partial_y\varphi\mathbf{y} \tag{A.10}$$

and that:

$$-Q^2\varphi + \partial_y^2\varphi + 4\pi\mathrm{i}(Q_x m_x + Q_z m_z) + 4\pi\partial_y m_y = 0. \tag{A.11}$$

In the following, we use the notations:

$$[f] = f(d) - f(0)$$

and $\langle f\rangle = \frac{1}{d}\int_0^d f(y)\,\mathrm{d}y$ (averaged value of f over the film thickness). Thus:

$$\langle\mathbf{h}\rangle = \mathrm{i}(Q_x\mathbf{x} + Q_z\mathbf{z})\langle\varphi\rangle + (1/d)[\varphi]\mathbf{y} \tag{A.12}$$

and:

$$-Q^2\langle\varphi\rangle + (1/d)[\partial_y\varphi] + 4\pi\mathrm{i}(Q_x\langle m_x\rangle + Q_z\langle m_z\rangle) + 4\pi(1/d)[m_y] = 0. \tag{A.13}$$

Noting by ψ the potential outside the film, the electromagnetic boundary conditions provide:

$$\partial_y\varphi(d) + 4\pi m_y(d) = \partial_y\psi(d), \qquad \varphi(d) = \psi(d) \tag{A.14}$$

and

$$\partial_y\varphi(0) + 4\pi m_y(0) = \partial_y\psi(0), \qquad \varphi(0) = \psi(0). \tag{A.15}$$

The potential ψ is a solution of:

$$-Q^2\psi + \partial_y^2\psi = 0. \tag{A.16}$$

Thus:

$$\psi = \psi_1\exp(\mathrm{i}(Q_x x + Q_z z) - Qy) \qquad \text{for } y > d \tag{A.17}$$

and

$$\psi = \psi_2\exp(\mathrm{i}(Q_x x + Q_z z) + Qy) \qquad \text{for } y < 0. \tag{A.18}$$

It results from relations (A.14)–(A.18) that:

$$[\partial_y\varphi] + 4\pi[m_y] + Q(\varphi(d) + \varphi(0)) = 0 \tag{A.19}$$

and

$$(\partial_y\varphi(d) + \partial_y\varphi(0)) + 4\pi(m_y(d) + m_y(0)) + Q[\varphi] = 0. \tag{A.20}$$

We consider slightly varying dynamical quantities over the thickness and, *consequently*, we use the approximation:

$$(m_y(d) + m_y(0)) \approx 2\langle m_y\rangle \tag{A.21}$$

$$(\varphi(d) + \varphi(0)) \approx 2\langle\varphi\rangle \tag{A.22}$$

and, hence:

$$(\partial_y\varphi(d) + \partial_y\varphi(0)) \approx 2\langle\partial_y\varphi\rangle = (2/d)[\varphi]. \tag{A.23}$$

The last three equations, combined with (A.13), (A.19) and (A.20), provide:

$$\langle\varphi\rangle = 4\pi\mathrm{i}(Q_x\langle m_x\rangle + Q_z\langle m_z\rangle)/(Q(Q + 2/d)) \tag{A.24}$$

$$[\varphi] = -8\pi\langle m_y\rangle/(Q + 2/d). \tag{A.25}$$

Thus:

$$\langle \mathbf{h} \rangle = -4\pi(Q_x \mathbf{x} + Q_z \mathbf{z})(Q_x \langle m_x \rangle + Q_z \langle m_z \rangle)/(Q(Q + 2/d)) - 8\pi \langle m_y \rangle/(dQ + 2)\mathbf{y}. \quad \text{(A.26)}$$

Finally, the components of $\langle \mathbf{h}_{\text{eff}} \rangle$ are:

$$\begin{aligned}
\langle h_{\text{eff},x} \rangle &= -4\pi Q_x (Q_x \langle m_x \rangle + Q_z \langle m_z \rangle)/(Q(Q + 2/d)) - H_a \langle m_x \rangle / M - 2AQ^2 \langle m_x \rangle / M^2 \\
\langle h_{\text{eff},y} \rangle &= -8\pi \langle m_y \rangle/(d(Q + 2/d)) - 2AQ^2 \langle m_y \rangle / M^2 \\
\langle h_{\text{eff},z} \rangle &= -4\pi Q_z (Q_x \langle m_x \rangle + Q_z \langle m_z \rangle)/(Q(Q + 2/d)) - 2AQ^2 \langle m_y \rangle / M^2.
\end{aligned} \quad \text{(A.27)}$$

Using these values in equation (A.5), one obtains the appropriate homogeneous system of linear equations, which provides the eigenfrequency given in equation (A.6).

References

[1] Jorzick J, Demokritov S O, Mathieu C, Hillebrands B, Bartenlian B, Chappert C, Rousseaux F and Slavin A N 1999 *Phys. Rev.* B **60** 15194
[2] Chérif S-M, Roussigné Y and Moch P 1999 *Phys. Rev.* B **59** 9482
[3] Chérif S-M, Roussigné Y, Dugautier C and Moch P 2000 *J. Magn. Magn. Mater.* **222** 337
[4] Roussigné Y, Chérif S-M, Dugautier C and Moch P 2001 *Phys. Rev.* B **63** 134429
[5] Jorzick J, Demokritov S O and Hillebrands B 2001 *J. Appl. Phys.* **89** 7091
[6] Guslienko K Y, Demokritov S O, Hillebrands B and Slavin A N 2002 *Phys. Rev.* B **66** 132402
[7] Jorzick J, Demokritov S O, Hillebrands B, Bailleul M, Fermon C, Guslienko K, Slavin A N, Berkov D and Gorn N L 2002 *Phys. Rev. Lett.* **88** 47204
[8] Roussigné Y, Chérif S-M and Moch P 2003 *J. Magn. Magn. Mater.* **263** 289
[9] Bailleul M, Fermon C, Olligs D and Demokritov S O 2001 *Europhys. Lett.* **56** 741
[10] Bayer C, Wang H, Yan M, Campbell C E and Crowell P A 2004 *Phys. Rev.* B **69** 134401
[11] Roussigné Y, Chérif S-M and Moch P 2004 *J. Magn. Magn. Mater.* **268** 89
[12] Roussigné Y, Chérif S-M and Moch P 2004 *J. Phys.: Condens. Matter* **16** 4591
[13] Kostylev M P, Stashkevitch A A, Sergeeva N A and Roussigné Y 2004 *J. Magn. Magn. Mater.* **278** 397
[14] Kostylev M P, Stashkevich A A and Sergeeva N A 2004 *Phys. Rev.* B **69** 064408
[15] Gubbiotti G, Kostylev M, Sergeeva N, Conti M, Carlotti G, Ono T, Slavin A N and Stashkevich A 2004 *Phys. Rev.* B **70** 224422
[16] Roussigné Y and Moch P 2005 *J. Phys.: Condens. Matter* **17** 1645
[17] Chérif S-M, Roussigné Y, Moch P and Sergeeva N A 2005 *J. Appl. Phys.* **98** 063905
[18] Gubbiotti G, Carlotti G, Ono T and Roussigné Y 2006 *J. Appl. Phys.* **100** 023906
[19] Chérif S-M and Hennequin J-F 1997 *J. Magn. Magn. Mater.* **165** 504
[20] Grimsditch M, Malozemoff A and Brunsch A 1979 *Phys. Rev. Lett.* **43** 711
[21] Camley R E, Raman T S and Mills D L 1981 *Phys. Rev.* B **23** 1226
[22] Cottam M G 1983 *J. Phys. C: Solid State Phys.* **15** 1573
[23] Roussigné Y, Ganot F, Dugautier C, Moch P and Renard D 1995 *Phys. Rev.* B **525** 30
[24] Rezende S M, Chesman C, Lucena M A, Azevedo A and Perkin S S P 1998 *J. Appl. Phys.* **84** 958
[25] Wee L, Stamps R L, Malinski L and Celinski Z 2004 *Phys. Rev.* B **69** 134426
[26] Stamps R L and Hillebrands B 1991 *Phys. Rev.* B **44** 12417
[27] Stamps R L 1994 *Phys. Rev.* B **49** 339
[28] Donahue M J, Porter D G, McMichael R D and Eicke J, Public code OOMMF URL: http://math.nist.gov/oommf